

High Thermoelectric Performance in Entropy Driven

$\text{Ge}_{1-2x-y}\text{Pb}_x\text{Sn}_x\text{Sb}_y\text{Te}$

Animesh Das, Paribesh Acharyya, Subarna Das and Kanishka Biswas*

New Chemistry Unit and School of Advanced Materials and International Centre for Materials Science Jawaharlal Nehru Centre for Advanced Scientific Research (JNCASR), Jakkur P.O., Bangalore 560064, India

**Email: kanishka@jncasr.ac.in*

Experimental details.

Reagents. Germanium (Ge, Strategic Metal, 99.999 %), tellurium (Te, Strategic Metal, 99.99 %), tin (Sn, Alfa Aesar, 99.99 %), lead (Pb, Alfa Aesar, 99.999 %) and antimony (Sb, Alfa Aesar, 99.9999 %) were used for synthesis of all the compounds.

Synthesis. High quality polycrystalline ingots (~8 g) of GeTe, $\text{Ge}_{1-2x}\text{Pb}_x\text{Sn}_x\text{Te}$, and $\text{Ge}_{0.84}\text{Pb}_{0.025}\text{Sn}_{0.025}\text{Sb}_{0.11}\text{Te}$ were prepared by mixing the stoichiometric amounts of high purity starting elements Ge, Te, Sn, Pb and Sb in quartz tubes followed by sealing under vacuum (10^{-6} Torr). The quartz tubes were slowly heated to 1223 K for 10 h, then soaked at 1223 K for 6 hours, followed by slow cooling to room temperature over 10 h. To ensure phase uniformity, the tubes in the furnace were shaken several times during dwelling at high temperature. In order to measure the electrical and thermal conductivity, ingot samples are cut into bars and coins respectively followed by smooth polishing of the surface. For further improvement of the zT, ball milling followed by Spark Plasma Sintering (BM+SPS) was performed in $\text{Ge}_{0.84}\text{Pb}_{0.025}\text{Sn}_{0.025}\text{Sb}_{0.11}\text{Te}$ sample. For that, the obtained ingot of $\text{Ge}_{0.84}\text{Pb}_{0.025}\text{Sn}_{0.025}\text{Sb}_{0.11}\text{Te}$ was crushed into fine powder and was ball milled in FRITSCH PULVERISSETTE 7 premium line planetary ball miller using stainless steel grinding bowls and balls for 150 minutes with a speed of 550 rpm. Ball milled powder was then consolidated into cylinder by spark plasma sintering (Dr. Sinter Lab, 211-LX) at 773 K and 50 MPa for 5 minutes.

Powder X-ray Diffraction (PXRD). Room temperature powder X-ray diffraction (PXRD) patterns for all the finely ground samples (GeTe, $\text{Ge}_{1-2x}\text{Pb}_x\text{Sn}_x\text{Te}$, ingot and ball milled $\text{Ge}_{0.84}\text{Pb}_{0.025}\text{Sn}_{0.025}\text{Sb}_{0.11}\text{Te}$) were recorded in a Rigaku Smartlab SE diffractometer using Cu $K\alpha$ radiation ($\lambda=1.5406 \text{ \AA}$). Rietveld refinement was performed using the FullProf program.¹

Transmission Electron Microscopy (TEM). TEM images of powder $\text{Ge}_{0.95}\text{Pb}_{0.025}\text{Sn}_{0.025}\text{Te}$ and $\text{Ge}_{0.84}\text{Pb}_{0.025}\text{Sn}_{0.025}\text{Sb}_{0.11}\text{Te}$ (BM) samples were taken using JEOL (JEM2100+) instrument (200 kV accelerating voltage). ThermoFisher Talos F200 S transmission electron microscope was used operating at 200 kV to analyze the structure and morphologies of $\text{Ge}_{0.84}\text{Pb}_{0.025}\text{Sn}_{0.025}\text{Sb}_{0.11}\text{Te}$ (BM+SPS) sample. TEM sample was prepared by (a) mechanical grinding, followed by precision ion polishing system (PIPS) to achieve thin (thickness 20 - 80 nm) foil, (b) drop casting ethanol solution of the sample in a Cu grid.

Field emission scanning electron microscopy (FESEM) in back-scattered electron (BSE) mode. FESEM-BSE images were taken using ZEISS Gemini SEM (500) – Field Emission Scanning Electron Microscope.

Thermal Conductivity. Thermal diffusivity, D , of the samples was measured directly by laser flash diffusivity method using Netzsch LFA-457 instrument in the 300–723 K temperature range under N_2 atmosphere. Coins with typical dimension of ~ 10 mm diameter and less than ~ 2 mm thickness were used for the measurements. Temperature dependent heat capacity, C_p , of GeTe was determined by comparing with a standard sample (pyroceram) in LFA-457 (Fig. S12). The total thermal conductivity, κ_T , was then estimated using the formula $\kappa_{\text{tot}} = D\rho C_p$, where ρ is the density of the samples which were found to be ~ 98 % of the theoretical value. The uncertainty in diffusivity (D) measurement is within 5%.

Electrical Transport. Temperature dependence of electrical conductivity (σ) and Seebeck coefficient (S) of the samples were measured simultaneously using a ULVAC-RIKO ZEM-3 instrument under helium atmosphere in the 300-723 K temperature range. The typical dimension of sample used for this measurement was $\sim 2 \times 2 \times 8 \text{ mm}^3$. The electrical and thermal transports were measured in same direction. The standard deviation of resistivity (ρ) and Seebeck coefficient (S), values are within 5% and 5%, respectively.

Hall Measurement. Room temperature carrier concentration were determined from Hall coefficient measurements with the instrument developed by Excel Instrument, India. The maximum applied magnetic field was 1T. Room temperature carrier concentration was estimated using the formula $1/e.R_H$, where e is the electronic charge and R_H is the Hall coefficient. The standard deviation of Hall coefficient (R_H) is within 5%.

Sound Velocity Measurement. The longitudinal (v_l) and transverse (v_t) sound velocities were measured on a disc-shaped sample by using an Epoch 650 Ultrasonic Flaw Detector (Olympus) instrument with the transducer frequency of 5 MHz. The mean sound velocity (v_m) was estimated using the formula²: $v_m = \left(\frac{3}{v_l^{-3} + 2v_t^{-3}}\right)^{\frac{1}{3}}$. The uncertainty in sound velocity measurement values is within 5%.

Device Fabrication. For fabrication of TE device, BM+SPS processed $Ge_{0.84}Pb_{0.025}Sn_{0.025}Sb_{0.11}Te$ and $Pb_{0.997}In_{0.003}Te_{0.996}I_{0.004}^3$ powder samples with layers of Fe/Cu at both ends were compacted via spark plasma sintering (SPS) technique to use them as p and n -type TE leg respectively. While for the p -type leg ($3.01 \times 2.89 \times 4.10 \text{ mm}^3$), SPS was done at 470 °C with 48 MPa for 5 min, n -type powder sample was compacted via SPS at 600 °C with 45 MPa for 5 min to fabricate the n -type leg ($2.58 \times 2.58 \times 4.10 \text{ mm}^3$). Fe was chosen to act as the diffusion barrier to hinder chemical reactions and element diffusion between TE materials and Cu layer. The legs were bonded to alumina based plates (thickness ~ 1 mm) with Cu interconnects. At the cold end, the legs were joined using In as soldering material. A Zn layer was used to connect both legs with Cu at the hot end. A schematic diagram of the fabricated device is shown in Fig. 6b. The performance of the TE device for power generation was evaluated by mini-PEM module testing system (Advance Riko).^{4,5}

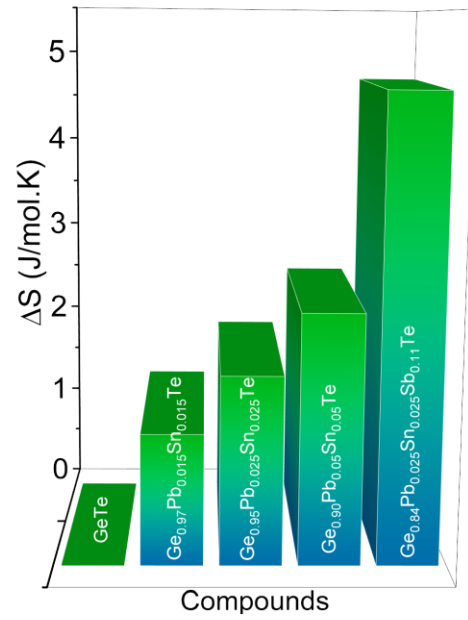


Fig. S1. The increase of configurational entropy at room temperature in GeTe based alloys.

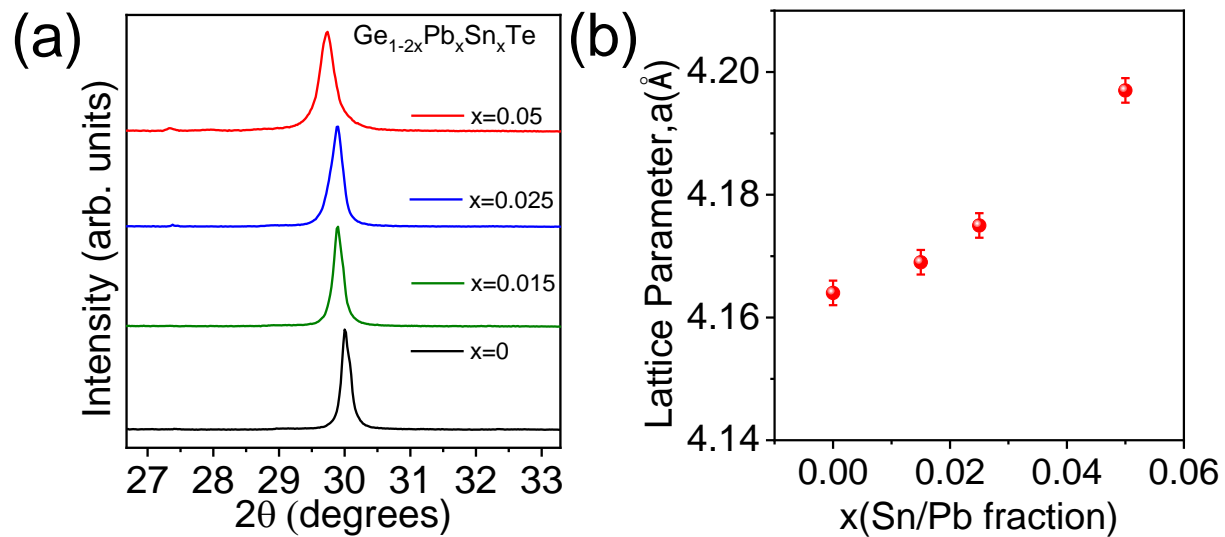


Fig. S2. (a) PXRD pattern of $\text{Ge}_{1-2x}\text{Pb}_x\text{Sn}_x\text{Te}$ ($x = 0 - 0.05$) samples showing the low angle shift of (202) Bragg peak due to incorporation of bigger Pb and Sn in GeTe, (b) Variation of lattice parameter (a in Å) of $\text{Ge}_{1-2x}\text{Pb}_x\text{Sn}_x\text{Te}$ ($x=0-0.05$) samples as a function of Pb/Sn concentration, x .

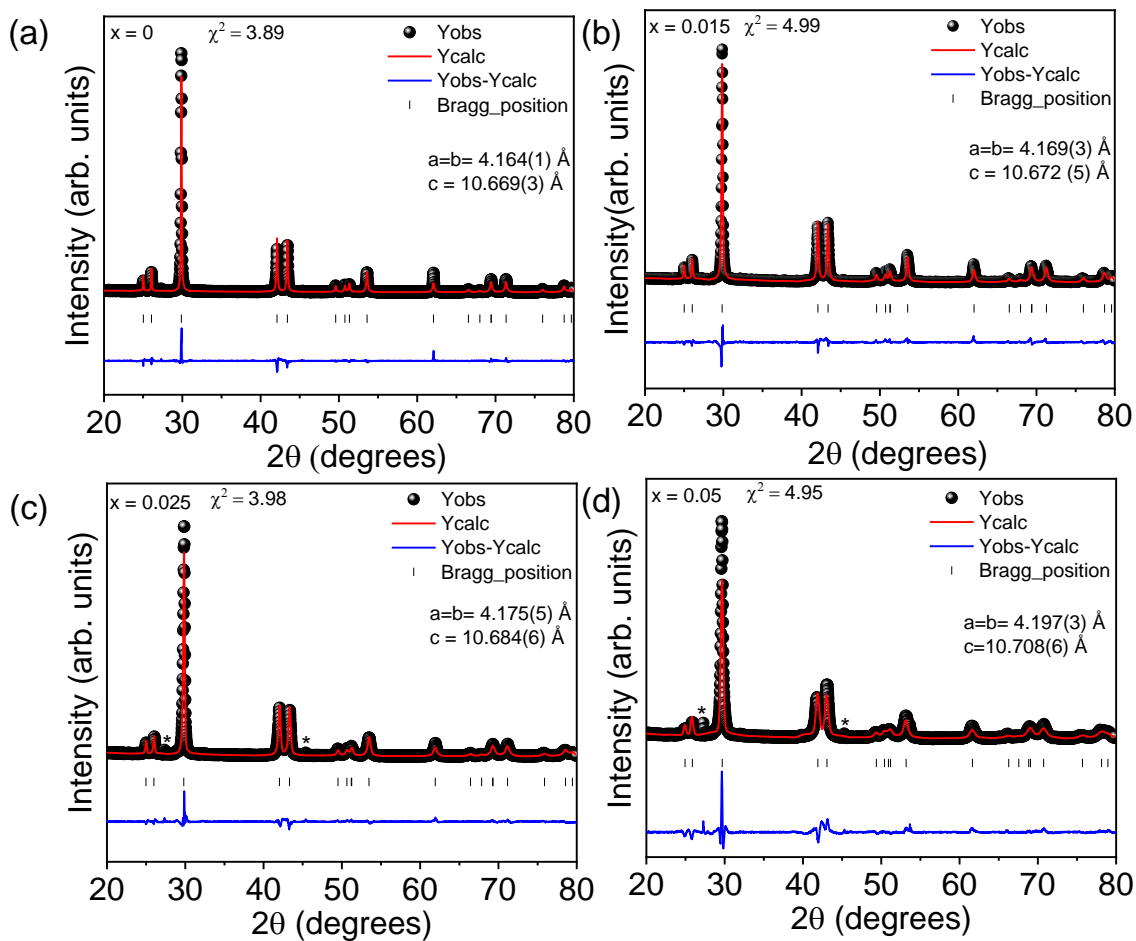


Fig. S3. Rietveld refinement based on PXRD data of ingot $\text{Ge}_{1-2x}\text{Pb}_x\text{Sn}_x\text{Te}$ i.e. (a) $x=0$, (b) $x=0.015$, (c) $x=0.025$, (d) $x=0.05$ samples fitted with $R3m$ phase of GeTe . (*) implies the presence of Ge impurity.

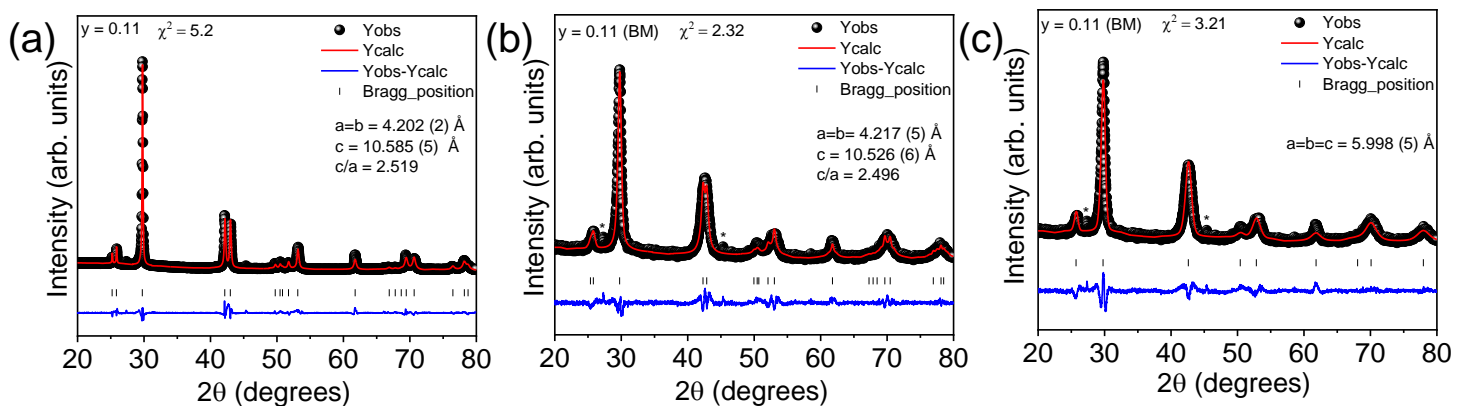


Fig. S4. Rietveld refinement based on PXRD data of (a) ingot $\text{Ge}_{0.95-y}\text{Pb}_{0.025}\text{Sn}_{0.025}\text{Sb}_y\text{Te}$ ($y=0.11$) fitted with $R3m$ phase of GeTe, (b) ball milled $\text{Ge}_{0.84}\text{Pb}_{0.025}\text{Sn}_{0.025}\text{Sb}_{0.11}\text{Te}$ fitted with $R3m$ phase of GeTe and (c) ball milled $\text{Ge}_{0.84}\text{Pb}_{0.025}\text{Sn}_{0.025}\text{Sb}_{0.11}\text{Te}$ sample fitted with $Fm\bar{3}m$ phase of GeTe. (*) implies the presence of Ge impurity.

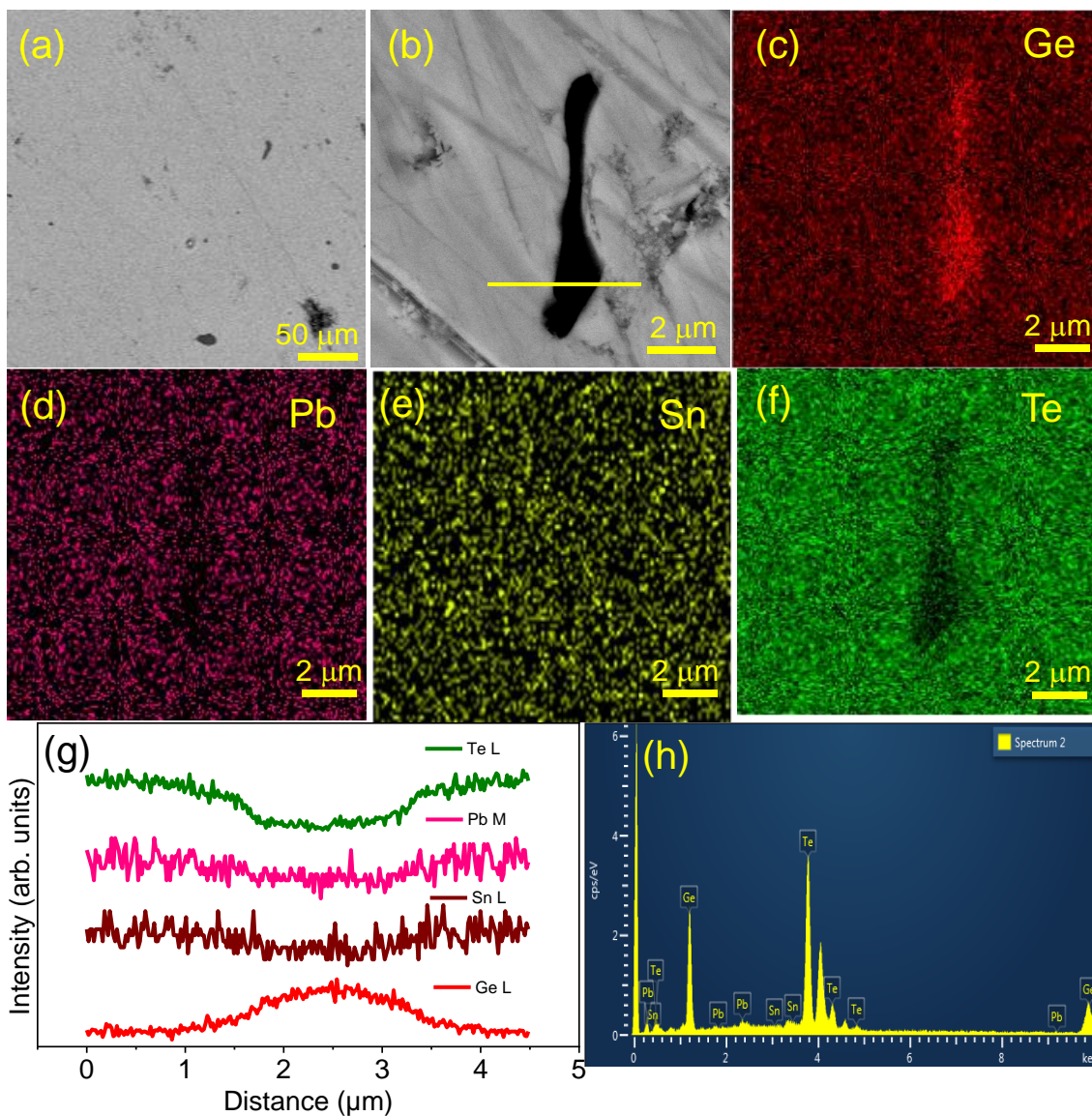


Fig. S5. (a and b) Backscattered FESEM images of different magnification, (c-f) EDS color mappings of $\text{Ge}_{0.95}\text{Pb}_{0.025}\text{Sn}_{0.025}\text{Te}$ ingot sample, (g) EDS line scanning along the precipitate as highlighted in (b) and (h) EDS spectrum of the matrix.

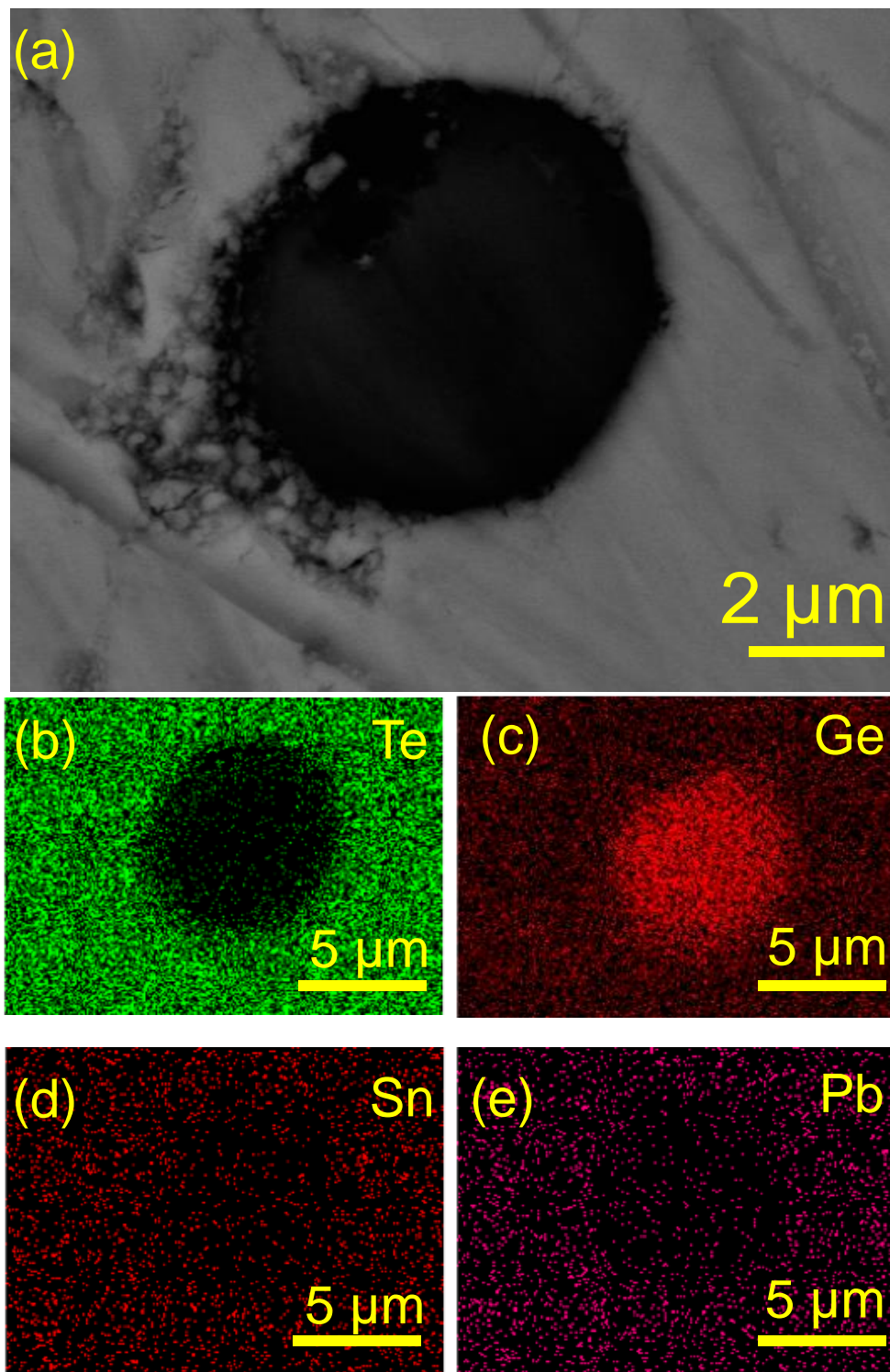


Fig. S6. (a) Backscattered FESEM images and (b-e) EDS color mappings of $\text{Ge}_{0.95}\text{Pb}_{0.025}\text{Sn}_{0.025}\text{Te}$ ingot sample.

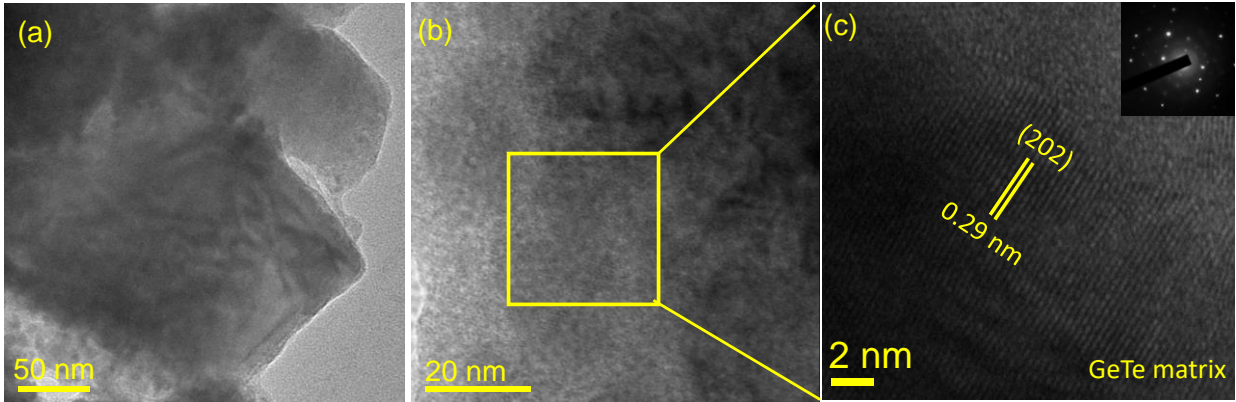


Fig. S7. TEM and HRTEM images of $\text{Ge}_{0.95}\text{Pb}_{0.025}\text{Sn}_{0.025}\text{Te}$ ingot sample. Inset of (c) shows the corresponding SAED pattern.

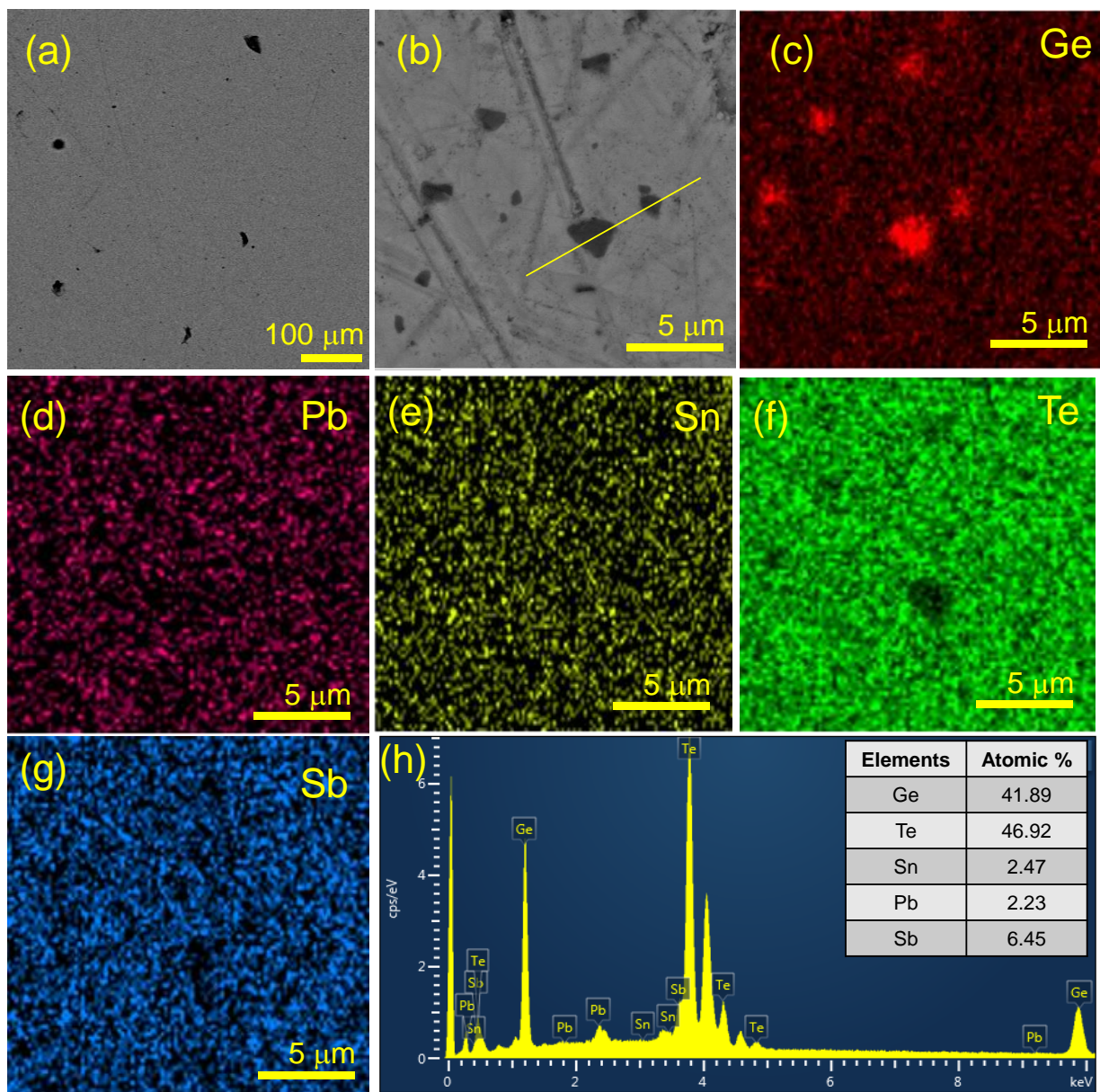


Fig. S8. (a and b) Backscattered FESEM images of different magnification, (c-g) EDS color mappings of $\text{Ge}_{0.84}\text{Pb}_{0.025}\text{Sn}_{0.025}\text{Sb}_{0.11}\text{Te}$ (BM+SPS) sample and (h) EDS spectrum of the matrix.

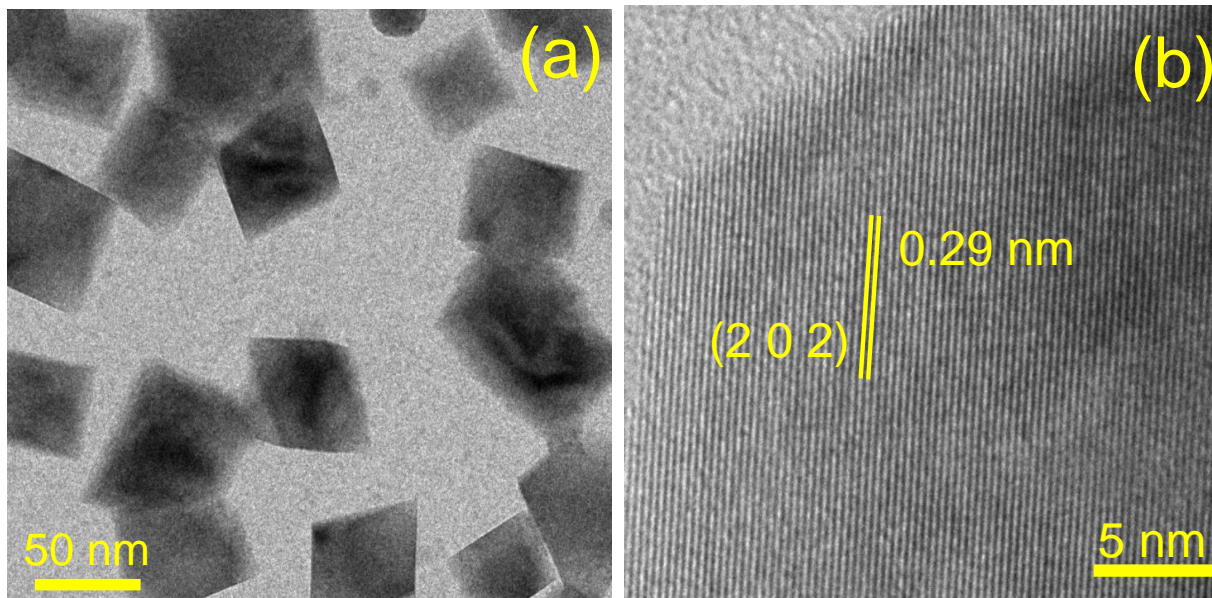


Fig. S9. (a) TEM image of $\text{Ge}_{0.84}\text{Pb}_{0.025}\text{Sn}_{0.025}\text{Sb}_{0.11}\text{Te}$ (BM) powder sample showing ~40-60 nm size particles and (b) HRTEM images showing d-spacing ~0.29 nm corresponding to (202) plane of $R3m$ GeTe.

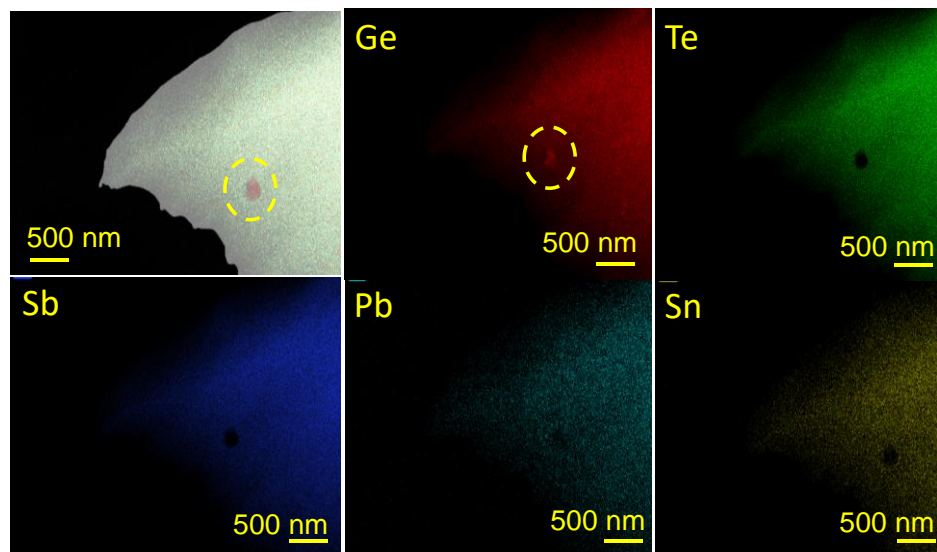


Fig. S10. EDS color mapping of $\text{Ge}_{0.84}\text{Pb}_{0.025}\text{Sn}_{0.025}\text{Sb}_{0.11}\text{Te}$ (BM+SPS) sample in STEM-HAADF mode indicating the presence of Ge nanoprecipitate.

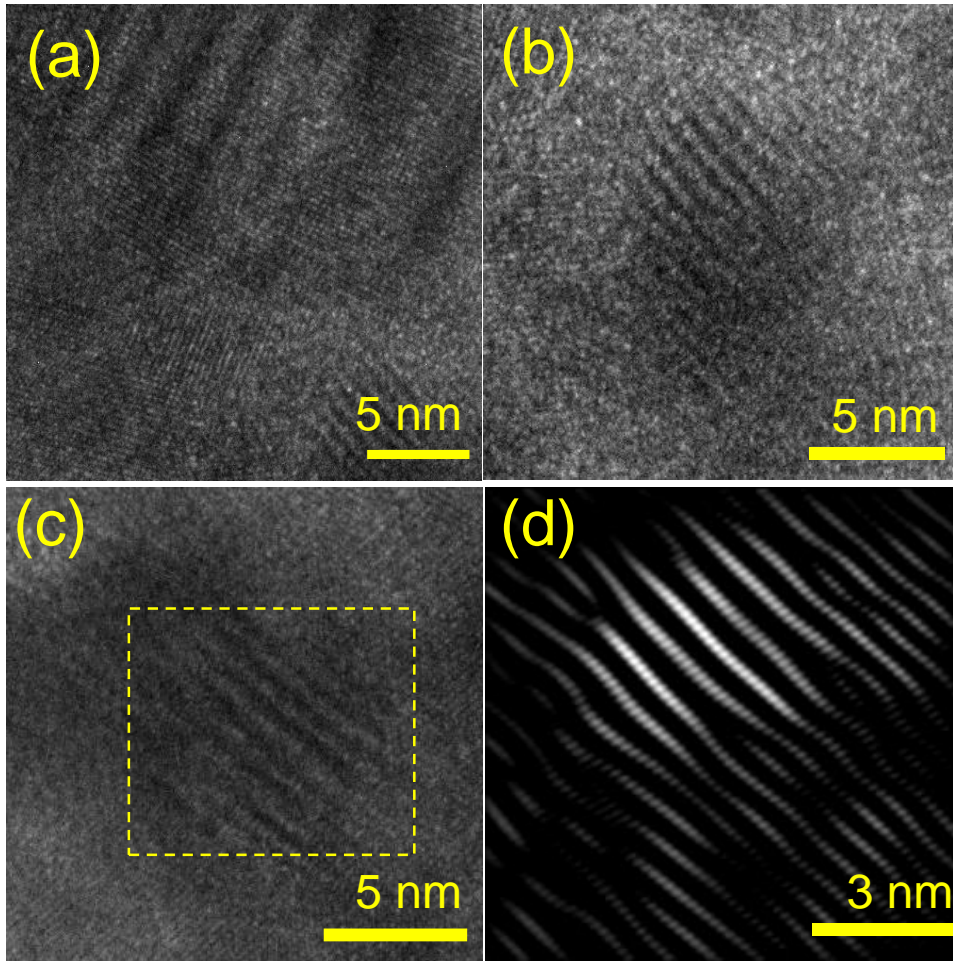


Fig. S11. (a, b and c) HRTEM images exhibiting presence of ripple like nanostructures in the $\text{Ge}_{0.84}\text{Pb}_{0.025}\text{Sn}_{0.025}\text{Sb}_{0.11}\text{Te}$ (BM+SPS) sample and (d) masked IFFT image of the selected region in (c) showing high-density dislocations.

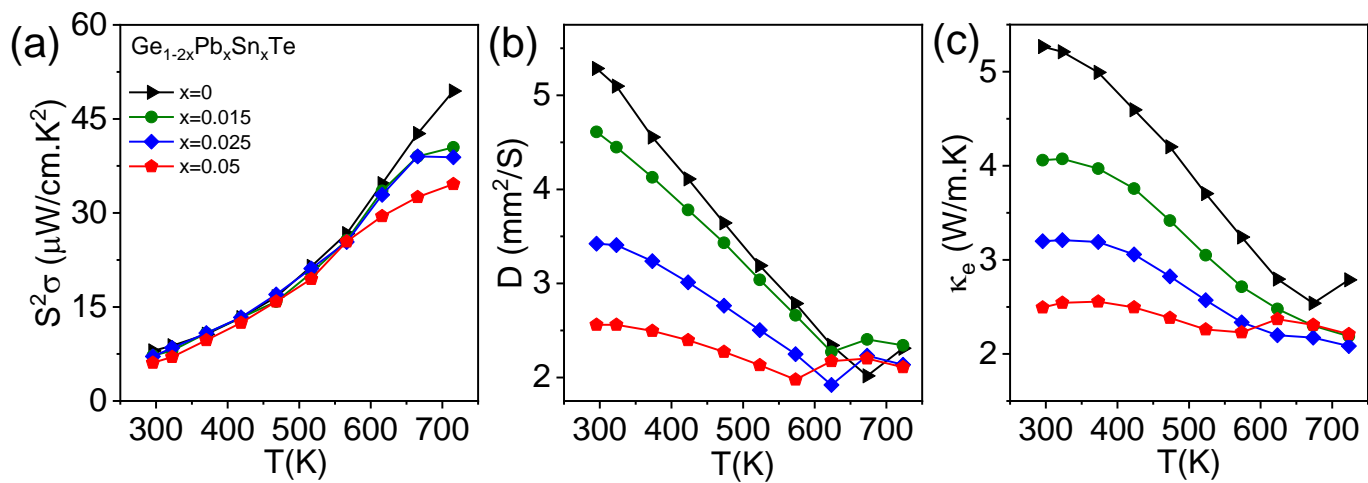


Fig. S12. Temperature dependent (a) power factor (σS^2), (b) thermal diffusivity (D) and (c) electrical thermal conductivity (κ_e) of $\text{Ge}_{1-2x}\text{Pb}_x\text{Sn}_x\text{Te}$ ($x = 0 - 0.05$) samples.

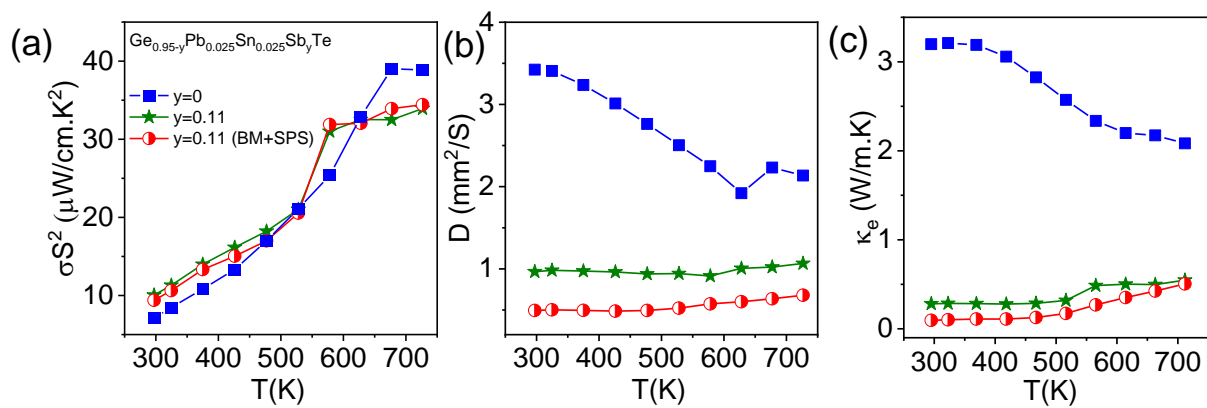


Fig. S13. Temperature dependent (a) power factor (σS^2), (b) thermal diffusivity (D) and (c) electrical thermal conductivity (κ_e) of ingot and BM+SPS $\text{Ge}_{0.84}\text{Pb}_{0.025}\text{Sn}_{0.025}\text{Sb}_{0.11}\text{Te}$ samples.

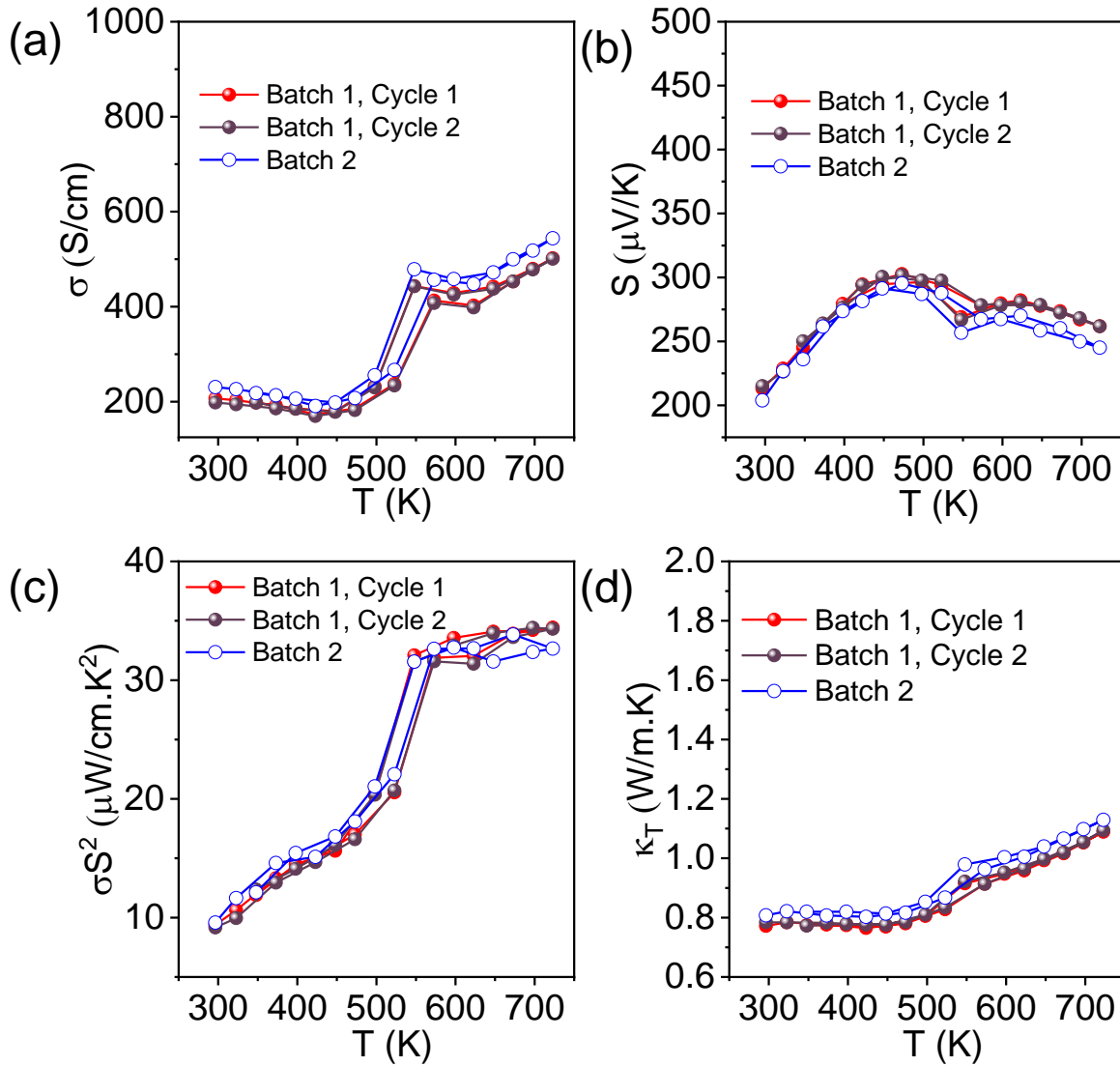


Fig. S14. Temperature dependent (a) electrical conductivity (σ), (b) Seebeck coefficient (S), (c) power factor (σS^2) and (d) total thermal conductivity (κ_T) of BM+SPS processed $\text{Ge}_{0.84}\text{Pb}_{0.025}\text{Sn}_{0.025}\text{Sb}_{0.11}\text{Te}$ sample showing reversibility and reproducibility over cycles and batches.

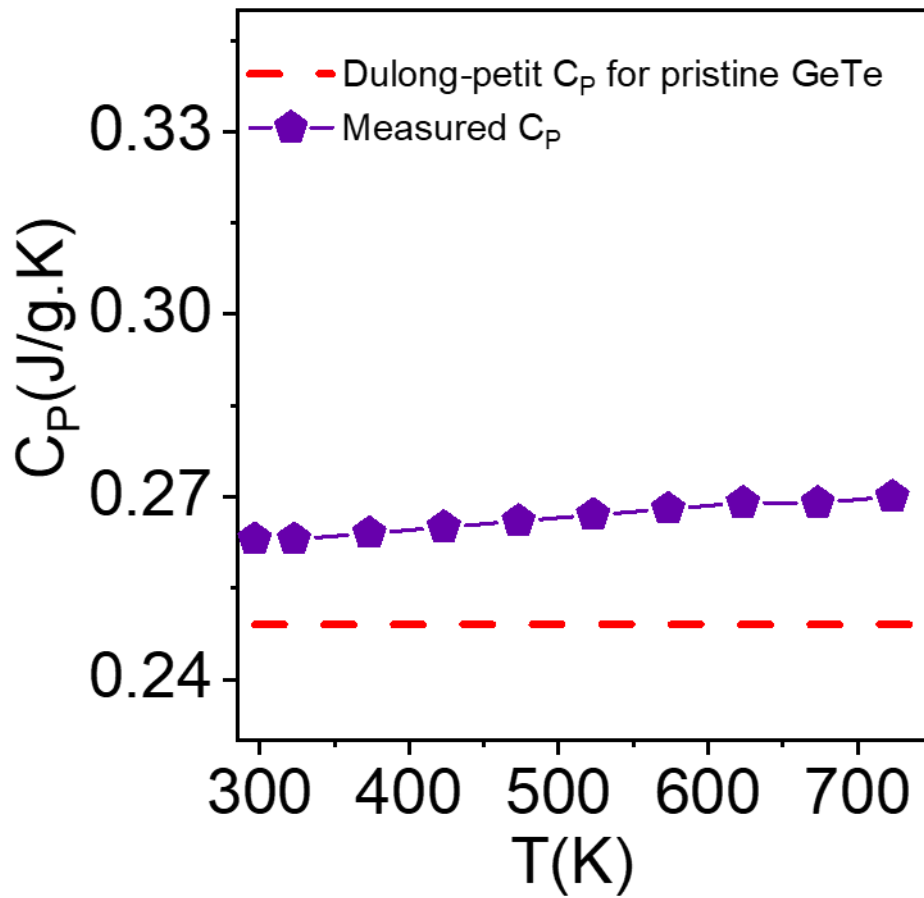


Fig. S15. Heat capacity at constant pressure (C_p) used to determine the total thermal conductivity (κ_T) for $\text{Ge}_{1-2x}\text{Pb}_x\text{Sn}_x\text{Te}$, ingot and BM+SPS processed $\text{Ge}_{0.84}\text{Pb}_{0.025}\text{Sn}_{0.025}\text{Sb}_{0.11}\text{Te}$ samples.

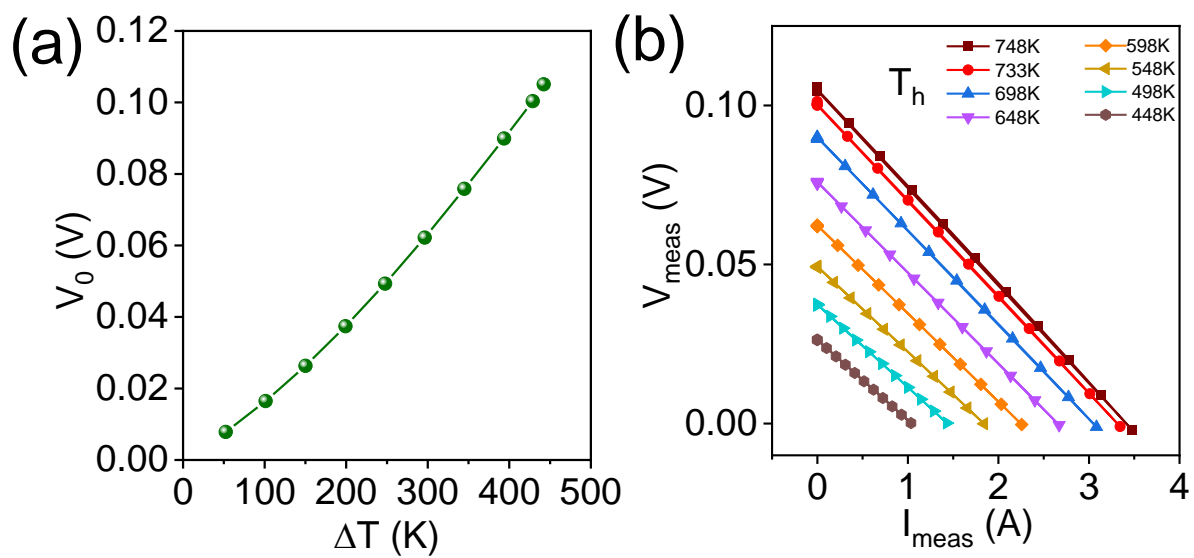


Fig. S16. Variation of (a) open circuit voltage V_0 (V) with ΔT and (b) measured voltage V_{meas} as a function of measured current I_{meas} of double leg thermoelectric device.

Table S1. Carrier concentration (n) and carrier mobility values (μ) of $\text{Ge}_{1-2x}\text{Pb}_x\text{Sn}_x\text{Te}$ samples.

Sample	n ($\times 10^{20}$)/ cm^3	μ (cm^2/Vs)
GeTe	7.0	71.9
$\text{Ge}_{0.97}\text{Pb}_{0.015}\text{Sn}_{0.015}\text{Te}$	6.2	58.5
$\text{Ge}_{0.95}\text{Pb}_{0.025}\text{Sn}_{0.025}\text{Te}$	6.1	48.0
$\text{Ge}_{0.90}\text{Pb}_{0.05}\text{Sn}_{0.05}\text{Te}$	5.9	40.9

Table S2. Callaway model fitting of lattice thermal conductivity (κ_L) of pristine GeTe and $\text{Ge}_{0.95}\text{Pb}_{0.025}\text{Sn}_{0.025}\text{Te}$ sample, where A is point defect prefactor and B is Umklapp scattering prefactor.

Sample	A [10^{-42} s^3]	B [$10^{-17} \text{ s K}^{-1}$]
GeTe	1.42	1.005
$\text{Ge}_{0.95}\text{Pb}_{0.025}\text{Sn}_{0.025}\text{Te}$	66.9	0.14

Table S3. Carrier concentration (n) and carrier mobility (μ) of $\text{Ge}_{0.84}\text{Pb}_{0.025}\text{Sn}_{0.025}\text{Sb}_{0.11}\text{Te}$ samples.

Sample	n ($\times 10^{20}$)/cm^3	μ (cm^2/Vs)
$\text{Ge}_{0.84}\text{Pb}_{0.025}\text{Sn}_{0.025}\text{Sb}_{0.11}\text{Te}$ (Ingot)	1.5	22.86
$\text{Ge}_{0.84}\text{Pb}_{0.025}\text{Sn}_{0.025}\text{Sb}_{0.11}\text{Te}$ (BM+SPS)	0.6	20.59

Table S4. Experimentally measured sound velocity of GeTe, Ge_{0.95}Pb_{0.025}Sn_{0.025}Te and Ge_{0.84}Pb_{0.025}Sn_{0.025}Sb_{0.11}Te (BM+SPS) samples.

Sample	Longitudinal sound velocity (m/s)	Transverse sound velocity (m/s)	Average sound velocity (m/s)
GeTe	3344	1946	2158
Ge _{0.95} Pb _{0.025} Sn _{0.025} Te	2942	1901	2086
Ge _{0.84} Pb _{0.025} Sn _{0.025} Sb _{0.11} Te (BM+SPS)	2312	1466	1612

Table S5. Variation of lattice parameter of $\text{Ge}_{0.95}\text{Pb}_{0.025}\text{Sn}_{0.025}\text{Te}$, ingot and ball milled $\text{Ge}_{0.84}\text{Pb}_{0.025}\text{Sn}_{0.025}\text{Sb}_{0.11}\text{Te}$ samples obtained from Rietveld refinement based on the PXRD data fitted with $R3m$ phase of GeTe.

Sample $\text{Ge}_{0.95-y}\text{Pb}_{0.025}\text{Sn}_{0.025}\text{Sb}_y\text{Te}$	c (Å)	a (Å)	c/a
y=0	10.684(6)	4.175(5)	2.559(4)
y=0.11 (ingot)	10.585(5)	4.202(2)	2.519(2)
y=0.11 (ball milled)	10.526(6)	4.217(5)	2.496(4)

References

1. T. Roisnel and J. Rodríguez-Carvajal, *Mater. Sci. Forum*, 2001, **378**, 118-123.
2. E. Rathore, R. Juneja, S. P. Culver, N. Minafra, A. K. Singh, W. G. Zeier and K. Biswas, *Chem. Mater.*, 2019, **31**, 2106-2113.
3. Q. Zhang, Q. Song, X. Wang, J. Sun, Q. Zhu, K. Dahal, X. Lin, F. Cao, J. Zhou, S. Chen, G. Chen, J. Mao and Z. Ren, *Energy Environ. Sci.*, 2018, **11**, 933-940.
4. P. Acharyya, S. Roychowdhury, M. Samanta and K. Biswas, *J. Am. Chem. Soc.*, 2020, **142**, 20502-20508.
5. S. Roychowdhury, T. Ghosh, R. Arora, M. Samanta, L. Xie, N. K. Singh, A. Soni, J. He, U. V. Waghmare and K. Biswas, *Science*, 2021, **371**, 722-727.